Cold electron scattering in SF_6 and C_6F_6: Bound and virtual state channels

D. Field,[1,*] N. C. Jones,[1] and J.-P. Ziesel[2]
[1]*Department of Physics and Astronomy, University of Aarhus, DK- 8000 Aarhus C, Denmark*
[2]*Laboratoire Collisions Agrégats Réactivité (CNRS UMR5589), Université Paul Sabatier, 31062 Toulouse, France*
(Received 26 November 2003; published 20 May 2004)

Experimental data are presented for the scattering of cold electrons by SF_6 and C_6F_6, down to energies of a few meV, with an energy resolution varying between 0.95 and 1.5 meV (full width at half maximum) in the electron beam. The measured scattering cross sections rise rapidly at low energy and represent effects of bound-state attachment and scattering in the case of SF_6 and virtual state scattering in the case of C_6F_6. Data are combined with known attachment cross sections for SF_6 to yield elastic-scattering cross sections, from which phase shifts for elastic scattering are derived. The *s*-wave phase shift rises as energy falls as theory requires for a potential supporting a nonadiabatic bound state and possessing a large positive *s*-wave scattering length. The behavior at very low energy of the *s*-wave phase shift is, however, anomalous, the phase shift remaining far from an odd multiple of π at 5 meV collision energy; a similar anomaly was found in electron scattering by CCl_4. These results should stimulate further theoretical development. By contrast with SF_6, C_6F_6 offers an example of a system with a large negative scattering length. Data are analyzed to reveal a strong virtual state effect at low collision energy, similar to CO_2 but with a considerably greater cross section. The *s*-wave phase shift falls as energy drops and both this and the *p*-wave phase shift follow the precepts of effective range theory. It is proposed that the strong virtual state effect may act as a gateway to attachment through collisional or radiative stabilization of long-lived anions, with implications for both man-made and natural plasmas.

DOI: 10.1103/PhysRevA.69.052716 PACS number(s): 34.80.−i

I. INTRODUCTION

Scattering and attachment of low-energy electrons by molecules display a variety of fundamental quantum phenomena such as virtual state scattering, giant resonances, Feshbach resonances, and shape resonances [1–9]. In the present work, we study electron collisions with SF_6 and C_6F_6, concentrating on the very-low-energy range of so-called "cold collisions," below 100 meV impact energy, in which the de Broglie wavelength of the electron is very much greater than the size of the target [10,11].

Both SF_6 and C_6F_6 attach electrons forming transient negative ions (TNIs) with lifetimes of several μs for C_6F_6, to perhaps as long as several ms for SF_6 [12]. The present data furnish an interesting comparison of these two molecular scattering systems, where in SF_6 a process of attachment takes place and, in C_6F_6, virtual state scattering.

The manner in which we assign a mechanism either of attachment or virtual state scattering is as follows. Consider first the case in which the nuclear nonadiabatic electron-molecule potential contains a bound state, that is, the electron-molecule surface connects with an electronically bound TNI without any relaxation of the nuclear framework. The encounter may then proceed via a process in which elastic scattering and attachment take place together in an interdependent manner [13,14]. This has been described for CCl_4 in [14] and also takes place in the present case for SF_6 [15]. In contrast to CCl_4 chemical reaction (dissociative attachment) in SF_6 to form $SF_5^- + F$, is thermodynamically forbidden at the low impact energies which concern us here [16], and an electron is eventually emitted.

For other molecular species, the nonadiabatic electron-molecule potential may not be sufficiently deep to contain an electronically bound negative-ion state. Scattering may then proceed via the single channel of virtual state scattering, as demonstrated recently for CO_2 [1]. For a significant virtual state effect, there should exist a nonstationary state of the negative ion which resides 1–2 eV, or generally even lower in energy, above the zero of energy of the neutral species. In the presence of the virtual state effect, long lifetimes of the TNIs may result for larger molecular species through coupling of the electron kinetic energy to nuclear motion within the TNI. This is the situation for low-energy electron collisions with C_6F_6.

The *s*-wave scattering length is a key quantity in characterizing cold collisions. From a viewpoint riding on the unperturbed matter wave associated with the impacting electron far from the target, the wave appears to have its origin in the vicinity of the target, either in front of or beyond it. The distance between the apparent origin of the wave and the target is defined as the scattering length and is to some degree equivalent to the radius of the target that the molecule presents to the incoming electron. If the apparent origin of the wave is in front of the target, then the scattering length is positive; if it is beyond the target, the scattering length is negative. A positive scattering length is associated with a bound state in the potential and a negative scattering length with a potential which is insufficiently deep to support a bound state. The present work concerns a pair of systems, one, SF_6, with a large positive scattering length, leading to electron attachment, and the other, C_6F_6, with a large negative scattering length, leading to virtual state scattering. The

*Corresponding author. Email address: dfield@phys.au.dk

study of these two molecules is essentially similar to tracing the behavior of a system as, through a theoretical construction, one allows a bound state in the interaction potential to rise, passing through zero energy, and move into the continuum, by making the potential increasingly shallow. In this sense, the present work echoes work in cold atom collisions involving magnetic tuning of the scattering length [10,17].

At the low energies studied here, collisions tend to be dominated by the *s*-wave, with some *p*-wave involvement, and by the asymptotic behavior of the scattering wave function for these partial waves, as manifested through the phase shift. To pursue the comparison of SF_6 and C_6F_6, we therefore derive phase shifts for the scattered electron partial waves. Theory is explicit on the issue of how these phase shifts should behave as a function of energy, e.g., [18]. For systems supporting a bound state, such as SF_6, with large positive *s*-wave scattering length, the *s*-wave phase shift should rise towards π (or some odd multiple of π) with decreasing collision energy. In virtual state scattering, such as in C_6F_6, with a large negative *s*-wave scattering length, the *s*-wave phase shift should by contrast fall with decreasing energy [1]. These results are based on highly idealized model potentials, for example a square well [18], with structureless spherical targets. As we find below and as we have seen in previous work on CO_2 [1], benzene [2], and CCl_4 [14], the essence of the physics turns out to be preserved to some degree within even such rudimentary quantum scattering descriptions.

The general process which we study involves electron attachment,

$$e^- + M \rightarrow M^{-*}, \quad M = SF_6, C_6F_6, \tag{1}$$

where M^{-*} eventually decays to the parent plus a free electron, or may be stabilized (or detached) by collision with the wall of the vacuum chamber in the experiment, or by other means (see Sec. V). The TNIs may transiently access states of the system in which the excess energy is distributed into motion within the nuclear framework, through electronic to nuclear kinetic energy transfer. Thus the anions M^{-*} will incipiently lower their electronic energy by channeling electronic energy into nuclear kinetic energy with accompanying rearrangement of the nuclear framework, as in low-energy electron scattering in CO_2 or CS_2 [1,7]. The nuclear motion accompanying this process may be coupled, in the present larger species, into the bath of inactive vibrations through "intramolecular vibrational relaxation" (IVR) [12,19]. Eventual recurrence of the energy into the initial mode(s) will cause detachment for both C_6F_6 and SF_6. However, as we have outlined above, the overall process for C_6F_6 may be viewed as elastic scattering via a virtual state, whereas for SF_6 the system undergoes attachment, but without chemical reaction.

II. PREVIOUS WORK: SF_6 AND C_6F_6

Electron scattering and attachment in SF_6 and C_6F_6 have been the subject of a very large number of investigations in recent years. A comprehensive review of the work involving SF_6 may be found in [16]. Data relevant to the present investigation are those for attachment cross sections in the few meV to tens of meV energy range, obtained from electron swarm data [16], Rydberg atom collisional data, e.g., [12,21], and in particular the (laser) threshold electron spectroscopy method developed by Chutjian and collaborators [22–25] and Hotop and collaborators [26–29] (see Sec. IV C 1). Total scattering data for SF_6 at low impact energies, the data reported here, are by contrast very scarce. There exists only one other study which reports data in the energy range of interest [30].

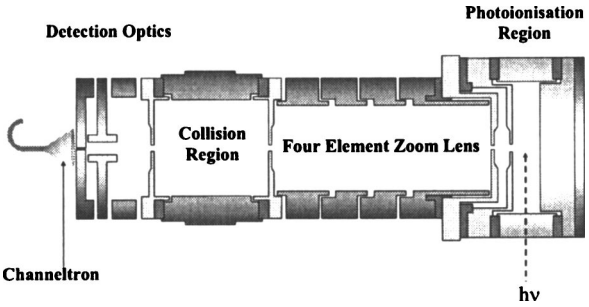

FIG. 1. A scale diagram of the apparatus. Monochromatic synchrotron radiation from ASTRID ($h\nu$) enters a photoionization region containing Ar. Photoelectrons, expelled by a weak electric field, are focused by a four-element lens [38] into a collision chamber containing the target gas. Transmitted electrons are detected at the channel electron multiplier (channeltron) situated beyond some further electron optics. The apparatus may be immersed in an axial magnetic field of 2×10^{-3} T.

Turning to C_6F_6 there are again numerous studies concerning $C_6F_6^-$ formation for very-low-energy electron impact or in collisions with Rydberg atoms. Relevant data may be found in [12,24,31–34]. Recent total and elastic electron scattering data may be found in [35,36]. There are, however, no data in the literature in the very-low-energy regime for comparison with the present work.

III. EXPERIMENTAL METHOD

The experimental system has been described in detail in [1,37] and is briefly outlined here. A schematic diagram of the system is shown in Fig. 1. Synchrotron radiation from the ASTRID storage ring at the University of Aarhus is focused into a cell containing Ar . Radiation is tuned to an energy two to three meV above the threshold for photoionization of Ar at 15.759 eV (78.676 nm [39]). The energy resolution of the photoelectrons is determined by the resolution in the photon beam via the performance of the beamline monochromator [37]. The resolution used in the present work varied between 0.9 and 1.25 meV full width at half maximum. Electrons are formed into a beam and pass through a room-temperature sample of SF_6 or C_6F_6. The intensity of the electron beam, in the presence and absence of target gas, is recorded at a channeltron as a function of electron energy. The cross section for electron-molecule encounters is derived via $\sigma_{T,I}=(Nl)^{-1}\ln(I_0/I_t)$, where N is the target gas number density, l is the path length in the gas, and I_0 and I_t are, respectively, the intensities of the incident and transmitted electron

beams. This yields the variation of the total integral scattering cross section, $\sigma_{T,I}$, where "total" refers to all events, elastic, inelastic, and reactive, and "integral" refers to integration over the full 4π sr.

In independent measurements, an axial magnetic field of strength $\sim 2\times 10^{-3}$ T is introduced. Under these conditions, electrons which are elastically scattered into the backward hemisphere are recorded as lost to the incident beam [37]. The scattering process imparts to these electrons velocities in the x and y directions, assigning the z-direction as the axial direction. As the backward-moving electrons pass through the lens system, they encounter transverse electric fields, E_x and E_y, around the boundaries between the lens elements. The resulting $E\times B$ force causes a trochoidal deviation in their paths and these electrons are lost by collisions with elements of the apparatus. Electrons that are forward scattered are picked up by the axial magnetic field and are guided onto the detector. These electrons do not therefore contribute to the measured cross section. The influence of long-lived TNIs is discussed in the section below.

The absolute electron energy scale is calibrated by observing the peak in the $N_2^-\ ^2\Pi_g$ resonance around 2.44 eV. Results in [40–42] indicate that the peak recorded in the total cross section at $\sim$2.44 eV is a good energy calibrator for both total and backward-scattering data, and thus for experiments with and without the magnetic field present. We assign an energy of 2.442 eV to this peak, this figure being the average of the values of 2.444 and 2.440 eV in [40] and [41], respectively. Discrepancies between the N_2 resonance energy and electron energies estimated from potentials in the system lay typically between 10 and 70 meV, and did not vary significantly over the course of many experiments. In the energy regime of a few tens of meV, reported values of electron energies are accurate to between ±1 and ±2 meV [11,37].

Uncertainties in the reported cross sections arise from sources including pressure measurements, random fluctuations in the electron beam intensities, and uncertainties in calibration of the path length of the electrons through the collision cell. These uncertainties correspond to an error of ±5% (one standard deviation) in the quoted cross sections at all energies for scattering in the presence or absence of the magnetic field, save at the very lowest energies in the absence of the magnetic field for which a figure of ±8% is appropriate.

Contributions to measured cross sections

We refer first to experiments involving the 2×10^{-3} T axial magnetic field. When electrons attach to the target species as in the present experiments, the TNIs may be sufficiently long-lived that they drift out of the line of sight defined by the entrance and exit holes of the scattering chamber. A long-lived TNI will be lost at the wall of the interaction chamber, 15 mm distant, or the electron may detach before this is achieved. In either case, once a sufficient drift has taken place, the experiment will record a loss in the transmitted electron current. Since the exit aperture of the collision chamber is 3 mm in diameter, a drift of $\geqslant$1.5 mm is sufficient that such a loss be recorded. $C_6F_6^-$, for example, drifts typically a distance of 1 mm in 6 μs. The most recent estimates, from Rydberg collisional data, suggest that for the lowest collision energies the TNI lifetime for the $C_6F_6^-$ species may extend into the range which would cause electron beam loss [12]. We find, however, no evidence this in our C_6F_6 data, as we discuss in Sec. IV D.

By contrast, we make the assumption in our subsequent analysis that SF_6^-, formed in the attachment channel below a few tens of meV impact energy, is sufficiently long-lived that the formation of all such species leads to loss of detected current. Thus we assume that when an electron has attached to SF_6, the TNI does not autodetach at sufficiently early times that the free electron would pass through the exit aperture of the collision chamber. This assumption is strongly supported by the considerable, if discrepant, literature values [12,43] (and references therein) for SF_6^- lifetimes. The most recent work suggests lifetimes between 20 μs [43]—which seem too short to account for observations, for example, in [16,26,44]—and $\sim$10 ms [12]. In connection with the above discussion, the trajectories of the product ions are not materially affected by the weak magnetic field in the system. In addition, the small average solid angles subtended by the apertures in the collision cell ensure that a negligible fraction of negative ions escape from the cell, in the presence or absence of the magnetic field.

On the basis of the above discussion, in the presence of the axial magnetic field, for SF_6, the measured cross section, $\sigma_{T,B}$, records the elastic (and inelastic) backward scattering cross section, into the backward 2π steradians, plus the integral cross section in the attachment channel. Hence for SF_6, $\sigma_{T,B}=\sigma_B^{\mathrm{el,inel}}+\sigma_I^{\mathrm{att}}$. For C_6F_6, the recorded cross section represents elastic (and any inelastic) backward scattering. Cross-section measurements in the absence of the magnetic field record the sum of the integral elastic, inelastic, and attachment cross sections, $\sigma_{T,I}=\sigma_I^{\mathrm{el,inel}}+\sigma_I^{\mathrm{att}}$, for SF_6 and the integral elastic and inelastic cross sections for C_6F_6.

The inelastic processes mentioned above may involve both vibrational and rotational changes. Vibrationally inelastic events are readily discernible in the data presented here for SF_6 (see Sec. IV A). Rotationally inelastic scattering is of very low cross section, since the molecules do not possess permanent dipole moments and there is no quadrupole moment for SF_6. Quadrupole induced transitions in C_6F_6 are of very low cross section [20] relative to the cross sections recorded here.

IV. RESULTS AND DISCUSSION

A. Experimental results for SF_6

Experimental data for scattering cross sections for SF_6 (purity $>$99.5%) are shown in Fig. 2 in the absence and in the presence of the axial magnetic field. Integral scattering cross sections have been recorded up to energies of 1 eV. The present data agree with the recommended values in [16] within better than 5% throughout the range 0.1–1 eV. At lower energies, the only available data for comparison are those of [16,30], which are in excellent agreement with our data at 0.1 eV and above, but tend progressively to be somewhat lower at energies below 0.1 eV, at worst 18% lower at

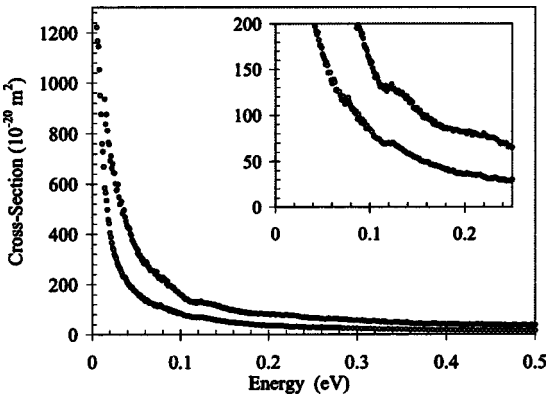

FIG. 2. SF_6 referring to data on the 0–0.5 eV energy scale. Upper set: the sum of the integral elastic, inelastic, and attachment cross sections, $\sigma_{T,I}$, measured in the absence of an axial magnetic field, between 14 and 500 meV. Lower set: the sum of the elastic backward scattering cross section, into the backward 2π steradians, and the integral cross section in the attachment channel, $\sigma_{T,B}$, obtained in the presence of the axial magnetic field, between 5 and 500 meV. The inset shows a blowup of the two data curves in the region where the influence of inelastic events may readily be discerned.

the lowest energies recorded in [30] of 36 meV. This discrepancy probably arises through the considerable difficulty in measuring the very low pressures required in those experiments, as mentioned in [30].

Data in the inset to Fig. 2 show the influence of vibrational excitation associated with the ν_3 IR-active mode at 117 meV [40,42]. These data serve as a useful additional absolute energy calibration since the Born-type process of ν_3 excitation has an onset at threshold [42].

B. Experimental results for C_6F_6

Experimental results for cross sections for C_6F_6 (Aldrich, $>$99.5%) are shown in Fig. 3 in the absence and in the presence of the axial magnetic field. Integral scattering cross sections have been recorded up to energies of 9.75 eV and may be obtained on request. The only data for which direct comparison can be made are those of [35]. Data between 2.9 and 9.75 eV agree within a few % with those reported here. However, at lower energies, increasing disagreement is encountered. Values of the integral cross section in [35] remain approximately constant at around 30 Å^2 down to the lowest energy recorded of 0.6 eV, whereas our values rise quite rapidly and at 0.6 eV achieve a figure of 100 Å^2 [45]). This discrepancy is compounded by the fact that in the same publication [35], the authors report total integral scattering cross sections for SF_6 which agree with the recommended data in [16] and thus with our data, down to energies of 0.6 eV.

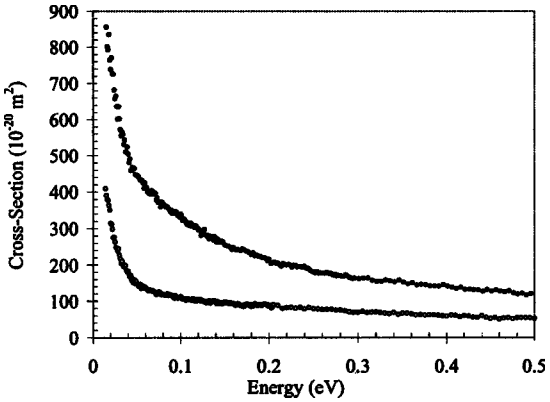

FIG. 3. C_6F_6: Upper set: the sum of the integral elastic and inelastic cross sections measured in the absence of an axial magnetic field, between 15 and 500 meV. Lower set: the elastic and inelastic backward scattering cross section, into the backward 2π steradians, obtained in the presence of the axial magnetic field, between 14 and 500 meV.

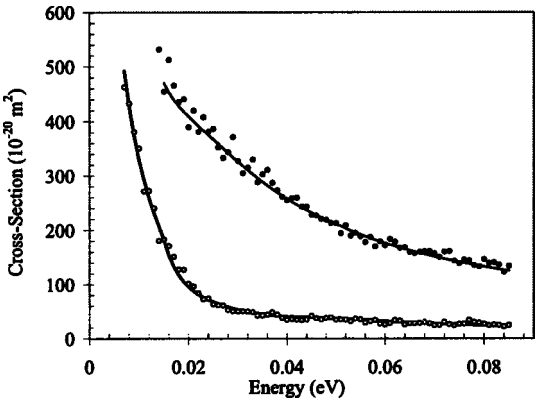

FIG. 4. SF_6: $\sigma_I^{\mathrm{el,inel}}$ (upper set) and backward $\sigma_B^{\mathrm{el,inel}}$ cross sections (lower set) for scattering of electrons by SF_6 as a function of electron impact energy. Errors in the cross sections are ±8% in $\sigma_I^{\mathrm{el,inel}}$ at the lowest energies, falling to ±5% at energies above $\sim$20 meV and ±5% in all $\sigma_B^{\mathrm{el,inel}}$. The solid lines show fits to these data, discussed in Sec. IV C 2.

C. Discussion of SF_6 data

1. Extraction of elastic-scattering data

Measurements have been made elsewhere of the variation of the cross section for attachment of electrons to SF_6, with an energy resolution comparable to that in the present experiment [16,26,44,46]. Recollecting that data in Fig. 2 represent $\sigma_{T,I}=\sigma_I^{\mathrm{el,inel}}+\sigma_I^{\mathrm{att}}$ (upper set) and $\sigma_{T,B}=\sigma_B^{\mathrm{el,inel}}+\sigma_I^{\mathrm{att}}$ (lower set), subtraction of attachment data in [26,44,46] from our data in Fig. 2 effectively yields the elastic cross sections for both integral and backward scattering [47]. In this connection, vibrational excitation is weak below the v_1 threshold at 95.4 meV (see Sec. IV C 2). The resulting cross sections are shown in Fig. 4.

In performing this simple subtraction, we implicitly adopt the model that there are essentially two groups of lifetimes involved in encounters of electrons with SF_6, short lifetimes (e.g., $<$ a few μs) associated with elastic scattering and long lifetimes associated with attachment. Thus we assume that in the presence of the magnetic field we obtain the backward scattering cross section on subtraction of the attachment cross section, without any contribution associated with long-lived TNIs. This assumption is nicely borne out by the ratios

of the backward to integral cross sections further discussed in Sec. IV C 2.

2. Analysis of elastic scattering data: SF_6

We set out to extract the *s*- and *p*- wave phase shifts from the experimental data in Fig. 4. The theory of collisions exhibiting both reaction and scattering has been described in [13,14]. The electron-molecule system is treated for elastic scattering and reaction in a central force field, that is, without reference to structure in the target. Thus the target is viewed as pointlike to the incoming long-wavelength de Broglie wave. Vibrational populations in the target lie at the few % level at 300 K and are neglected in the subsequent analysis.

A large number of theoretical calculations, reviewed in [16,46], with some recent additional calculations in Tachikawa [48], show that the lowest unoccupied molecular orbital (LUMO) of SF_6 is $6a_{1g}$. Thus SF_6^- has an electronic ground state $^2A_{1g}$, the negative ion maintaining the octahedral symmetry of the neutral. Only the *s*-wave has the A_{1g} symmetry of the LUMO under the operations of the octahedral (O_h) point group, and therefore only the *s*-wave is active in attachment.

Following [14], we use the standard expression for the scattering amplitude [49], and write the S matrix, S^l, for the lth partial wave, in the form

$$S^l = \epsilon_l \exp(2i\eta_l), \tag{2}$$

where ϵ_l are scattering matrix elements for attachment in the angular momentum representation [50]; thus ϵ_0 may be identified with $|S_0^2|$ in [50]. ϵ_l essentially dictate the relative importance of reaction and scattering as a function of energy. The cross section for elastic scattering, including only *s*- and *p*-waves, may then be shown to be

$$\sigma_{\text{elastic}} = \frac{\pi}{2k^2}[\epsilon_0^2 x_0^2 z + 3z^2\epsilon_0\epsilon_1 x_0 x_1 + 3z^3\epsilon_1^2 x_1^2 + w_0^2 z + 3z^2 w_0 w_1 + 3z^3 w_1^2], \tag{3}$$

where the cross section is evaluated between any chosen angles θ_1 and θ_2, where z is $\cos\theta$, $x_l = \sin 2\eta_l$, $w_l = 1 - \epsilon_l \cos 2\eta_l$, where $l=0$ or 1, for *s*- and *p*-waves, respectively, and the azimuthal angle has been integrated out. k is the magnitude of the wave vector, where $k=\sqrt{2E}$ (atomic units, $\hbar = m = e = 1$, are used throughout unless indicated otherwise).

It follows that the integral scattering cross section is given by [13,14]

$$\sigma_I^{\text{elastic}} = \frac{\pi}{k^2}[1 + \epsilon_0^2 - 2\epsilon_0 \cos 2\eta_0 + 3(1 + \epsilon_1^2 - 2\epsilon_1 \cos 2\eta_1)] \tag{4}$$

and the backward scattering cross section by

$$\sigma_B^{\text{elastic}} = \frac{\pi}{2k^2}\{1 + \epsilon_0^2 + \epsilon_0 \cos 2\eta_0 + 3[\epsilon_1^2 - \epsilon_1 \cos 2\eta_1 - \epsilon_0\epsilon_1 \cos 2(\eta_0 - \eta_1)]\}. \tag{5}$$

The integral attachment (or reaction) cross section is given by

$$\sigma_I^{\text{att}} = \frac{\pi}{k^2}[4 - \epsilon_0^2 - 3\epsilon_1^2]. \tag{6}$$

Since only *s*-wave attachment is allowed, $\epsilon_1 = 1$ in Eqs. (2)–(6) and values of ϵ_0 may be trivially derived, using Eq. (6), from experimental values of the attachment cross section [4,16,44,46]. We note that $\epsilon_1 = 1$ represents a limiting description of the encounter, since the LUMO of SF_6 is not strictly pure A_{1g} but may possess some admixtures of symmetries which may allow a weak *p*-wave interaction.

Equations (3)–(6) exemplify the interdependence of reactive and scattering channels, since ϵ_0, derived from attachment data, appears in the expressions for elastic scattering. This interdependence is introduced at the most fundamental level via the scattering amplitude and is essentially expressed in Eq. (2). This feature arises despite the fact that the two channels are very different in aspect, in the one case with the output channel characterized by a free scattered electron, with a short scattering state lifetime, and in the other associated with very long-lived SF_6^-. The interdependence of these disparate channels, which communicate at whatever physical range, represents a nice example of the peculiar nature of quantum scattering.

The above expressions may now be used to derive phase shifts for *s*- and *p*-waves for the elastic-scattering process in the presence of attachment, thus characterizing the collision process. We seek to fit simultaneously the integral and backward elastic scattering cross sections in Fig. 4 by choosing a suitable set of *s*- and *p*-wave phase shifts, η_0 and η_1 versus electron collision energy. This is achieved by expressing the phase shifts as polynomial expansions in k, and varying the coefficients of this expansion, as described in [1]. Expansions up to k^5 are adequate to extract values of η_0 and η_1 within the accuracy of the experimental data.

Fits were performed up to 85 meV, avoiding the Raman-active v_1 mode at 95.4 meV, which has a strong influence at threshold on the scattering behavior of SF_6, in inelastic, elastic, and attachment channels [16,26,42,44] and as we discuss further below. Results of fitting are shown in Fig. 4, which demonstrates that a good fit may be achieved with Eqs. (4) and (5) within the chosen energy range. *s*- and *p*-wave phase shifts corresponding to the fits in Fig. 4 are shown in Fig. 5. The analysis does not allow the determination of the sign of the phase shifts, but determines that they both possess the same sign. A positive sign is adopted. To any value of the phase shift one may also arbitrarily add any odd multiple of π. The *s*-wave phase shift rises as energy falls, as was found for electron collisions with CCl_4 [14] and as expected for a system possessing a bound state in the potential governing the collision [18]. The ratio of scattering to reaction cross section is a governing factor in the detailed behavior of the *s*-wave phase shift with energy. This ratio becomes constant within experimental error between 50 and 80 meV, and this is reflected in the constancy of η_0 in this energy range, as seen in Fig. 5.

A serious difficulty is encountered in understanding the *s*-wave phase shifts shown in Fig. 5. Since σ_I^{att} tends to a finite value as the energy tends to zero, then ϵ_0 must tend to unity as the collision energy approaches zero. It then follows, for internal consistency, that the phase shift must tend to an

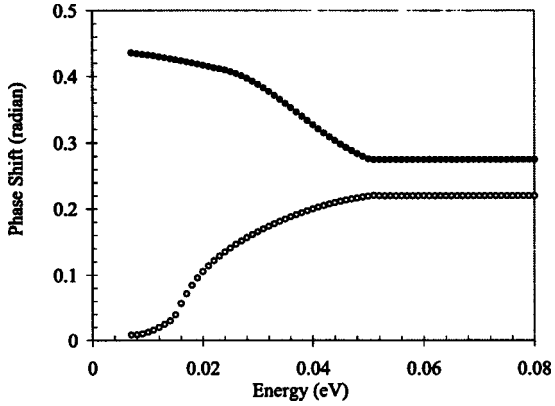

FIG. 5. *s*-wave (solid circles) and *p*-wave (open circles) phase shifts for $e^- + SF_6$ elastic scattering derived from fitting procedures, applied to data in Fig. 4, described in Sec. IV C 2. Errors in the phase shifts are ±5%.

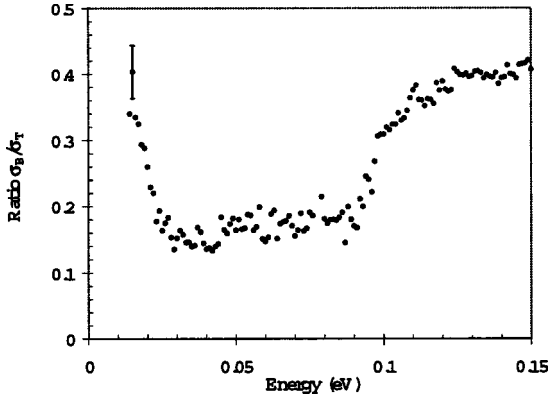

FIG. 6. SF_6: the ratio R of the backward scattering cross section to the integral scattering cross section obtained from data in Fig. 4, as a function of electron impact energy.

odd multiple of π at zero energy. However, our derived s-wave phase shifts do not show this. Very similar behavior was found for the analogous case of coupled reactive and elastic scattering in CCl_4 [14]. One explanation may be that the very-low-energy regime, which should show $\eta_0 \rightarrow \pi$, lies below a few meV collision energy, a regime which we are unable to probe. Alternatively, and in addition, our analysis is based on a purely electronic description of the interaction, in which there is no coupling between electronic and nuclear kinetic energy in the asymptotic input and output channels. The anomalous behavior of the *s*-wave phase shift in Fig. 5 may represent the breakdown of this purely electronic model at the low energies encountered here, with coupling between the electronic and nuclear degrees of freedom. In this case, this would be principally through the a_{1g} breathing mode, as discussed in detail, for example, in [19] for nondissociative electron attachment to SF_6.

We can, however, show that our data do not exclude the result that the *s*-wave phase shift may approach π as energy tends to zero. The attachment cross section at an impact energy of 0.1 meV has been measured to be 7617 $Å^2$ [44,46], yielding $\epsilon_0 = 0.9677$. Extrapolation of the elastic data in Fig. 4 to zero energy suggests a limiting integral cross section of between 1000 and 2000 $Å^2$. If we insert these values into Eq. (4) and use $\eta_1 = 0.0087$, the value obtained by fitting at 8 meV, we then find $\eta_0 \sim (\pi - 0.05) \pm 0.01$ for a collision energy of 0.1 meV, that is, η_0 is very close to an odd multiple of π.

The variation of the *p*-wave phase shift at low energy provides further evidence that we are dealing with a coupled-channel scattering problem rather than with a single-channel problem. Single-channel scattering is well-described by modified effective range theory (MERT [51]), especially at energies as low as a few tens of meV. MERT requires that the *p*-wave phase shift decrease approximately linearly with energy at low energy [see Eq. (9), Sec. IV D 2]. Linearity is not encountered in the variation of the *p*-wave phase shift shown in Fig. 5. Similar behavior to that in Fig. 5 was found for the variation of the *p*-wave phase shift with energy in the case of CCl_4 [14], in which attachment also takes place and which again is a coupled-channel system. The present results, and those in [14], are in contrast to single-channel scattering in C_6F_6, Sec. IV D 1, which exhibits regular effective range behavior. To underline this distinction between single- and coupled-channel scattering, we have imposed the condition that η_1 varies as k^2 below 30 meV in analyzing the SF_6 data in Fig. 4. When this restriction is applied, it is found that it is no longer possible to find a set of *s*- and *p*-wave phase shifts which fit both backward and integral elastic cross sections to within the experimental error in our data. This is in contrast to the first shown in Fig. 4.

As we have just noted and as described in [14], one cannot strictly consider elastic scattering independently of attachment because of the coupled nature of the scattering. Nevertheless, it turns out to be instructive to consider the ratio of the backward to integral scattering cross section, *R*, in SF_6 using data in Fig. 4. This ratio is shown in Fig. 6 as a function of electron impact energy. A useful check on our data is that the ratio tends to 0.5, within the errors, at zero energy. This provides good evidence that the cross section measured in the presence of the axial magnetic field is the backward elastic scattering cross section (after subtraction of the attachment contribution), without any significant contribution from SF_6^- of lifetimes longer than ~7.5 μs. The very rapid rise below 30 meV from strong forward scattering with $R \sim 0.175$ to much more nearly backward-forward symmetric scattering is reflected in the sharp drop in the *p*-wave phase shift in this energy range (Fig. 5). Strong forward scattering persists up to the energy for the threshold for v_1 excitation. As described in [42], interactions involving the v_1 Raman-active a_{1g} mode, at 95.4 meV, take place through the *s*-wave attachment channel, the molecule expanding as the anion forms, mimicking the a_{1g} breathing vibration. This enhances the *s*-wave scattering channel, and the ratio *R* rises sharply. The vibrational resonance at a threshold of 117 meV, corresponding to the $v_3\ t_{1u}$ IR-active vibration (see the inset to Fig. 2), involves impulsive excitation by $p_{x,y,z}$ on the input channel and s-waves on the output channel, or vice versa [42]. The net result appears to have little influence on the value
of *R*.

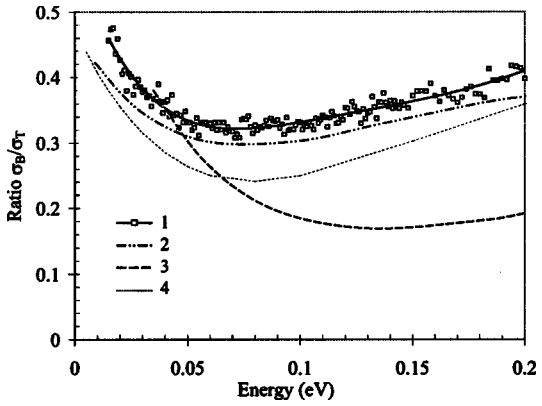

FIG. 7. 1, C_6F_6: the ratio R of the backward scattering cross section to the integral cross section as a function of electron impact energy, obtained from data in Fig. 3. The line through the experimental data has been drawn to guide the eye. 2, the variation of R for CO_2; see [1]. 3, the variation of R for C_6D_6; see [2]. 4, a theoretical estimate of the variation of R for C_6H_6; see [2].

D. Discussion of C_6F_6 data

We treat electron interactions with C_6F_6 as scattering via a virtual state. In this connection, we see no evidence in our data for beam loss due to long-lived TNIs in the presence of the axial magnetic field (as mentioned in Sec. III), despite the long lifetimes of at least 200 μs reported for 10–15% of C_6F_6 TNIs [12]. This is demonstrated in Fig. 7, which shows that the ratio *R* tends to 0.5, within experimental error, as the electron impact energy tends to zero. Hence cross sections measured in the presence of the axial magnetic field are pure backward scattering cross sections.

The calculations of the potential energy surface for C_6F_6 reported in [52] show that if $C_6F_6^-$ retains D_{6h} symmetry, the TNI is then unbound relative to C_6F_6. The $^2A_{1g}$ state of the TNI, which is the ground state of the anion in D_{6h} symmetry, (without any nuclear rearrangement), is calculated to lie 56 meV above the energy of the neutral. We propose that the electron is captured directly into this unbound state and is eventually expelled (detached) via this gateway. Hence the conditions for scattering are those of virtual state scattering. In the interior region in which long-lived $C_6F_6^-$ dwells, considerable coupling takes place between electronic and nuclear motion. Using the calculation in [52] as a guide, the s wave enters to form the $^2A_{1g}$ state of the TNI, as suggested above. Electronic-nuclear coupling distorts the nuclear framework in the absence of electronic degeneracy through so-called pseudo-Jahn-Teller coupling. This acts via the e_{2u} C–H and C-C-C bending vibrations and transforms the system into the C_{2v} and D_2 states. These are, respectively, bound by 356 and 347 meV [52] and are the two most strongly bound states of the anion. Various other geometries within the potential surface are also bound (Table 3 of [52]) and the overall picture is one in which there is substantial phase space associated with electronic bound states accompanied by rearrangement of the nuclear framework. We return to this when we discuss the vibrational states of the target in Sec. IV D 3.

In connection with the above discussion, the absolute accuracy of the energies of states recorded in [52] is difficult to assess since experimental values of the adiabatic electron affinity range between 0.5 and 0.8 eV [33,53–55]. This spread of values may be compared with the theoretical value of ~0.35 eV in [52], small differences in zero-point energies apart.

1. Analysis of elastic scattering data: C_6F_6

Proceeding on the basis that the scattering is virtual state n nature, *s*- and *p*-wave phase shifts are derived below. The method of analysis is essentially the same as for electron scattering by CO_2 [1]. We assume that *s*- and *p*-partial waves make the principal contribution to the scattering, a good approximation at low energies. We have, however, included *d*-waves to check that the contribution is indeed very small. The assumption is also made that the long-range interaction potential of electrons with C_6F_6 is spherically symmetrical (see also Sec. IV D 2). This approximation breaks down at sufficiently long range due to the angle-dependent charge-permanent quadrupole interaction. Using a value of the quadrupole moment of -5 ± 0.25 a.u. [56,57], one may show that the quadrupole interaction becomes comparable with the charge-induced dipole interaction at a range of ~50 a.u. Since this corresponds to a cross section of ~2400 Å^2 which is considerably larger than cross sections measured here (see Fig. 3), the assumption of a spherically symmetrical potential is acceptable. Thus, without any additional assumptions about the radial dependence of the electron-C_6F_6 interaction potential, the elastic scattering cross section integrated between the two angles θ_1 and θ_2 [58], including only terms for $l=0$, 1, and 2, may be expressed as

$$\sigma(\theta_1,\theta_2)=\frac{2\pi}{k^2}\Bigg[b_0 z+3z^2\left(b_0b_1+\frac{b_0b_1}{4}\right)+5z(z^2-1)\left(b_0b_2+\frac{c_0c_2}{4}\right)+3b_1z^3+\frac{25}{4}b_2\left(\frac{9z^2}{5}-2z^3+z\right)+\frac{15}{2}z^2\left(\frac{3z^2}{2}-1\right)\left(b_1b_2+\frac{c_1c_2}{4}\right)\Bigg]_{\theta_1}^{\theta_2}, \quad (7)$$

where $z=\cos\theta$, $b_l=\sin^2\eta$, and $c_l=\sin 2\eta_l$. For backward scattering, $\theta_2=\pi/2$ and $\theta_1=\pi$, and for integral scattering, $\theta_2=0$ and $\theta_1=\pi$.

In order to extract phase shifts, we have expressed these as expansions in *k*, as in analysis of the SF_6 data, Sec. IV C 2. As in SF_6 expansions up to k^5 are adequate to extract values of η_0, η_1, and η_2 within the accuracy of the experimental data. The coefficients of powers of k in expansions for *s*- and *p*-wave phase shifts have been varied so as to reproduce as closely as possible our experimental data on a least-squares basis, using Eq. (7). This simple fitting procedure, "partial-wave fitting," yields a set of absolute values of *s*- and *p*-wave phase shifts, modulo π, as a function of impact energy. In order to limit the inaccuracy associated with inclusion of only low partial waves, data were fitted to energies no higher than 50 meV. Fits are shown in Fig. 8 and the corresponding phase shifts in Fig. 9. *d*-wave phase shifts, not

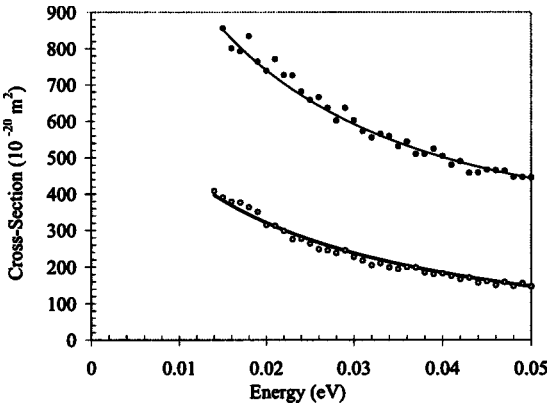

FIG. 8. C_6F_6: fits to experimental data obtained using Eq. (7). Fits are shown as continuous lines, experimental data for integral cross sections as full circles, and backward scattering cross sections as open circles.

shown in Fig. 9, are consistently an order of magnitude smaller than *p*-wave phase shifts.

Results in Fig. 9 show the strong and increasing dominance of the *s*-wave at lower energy. Thus at 50 meV impact energy, the *s*-wave contributes 94.5% of the integral cross section, a figure which rises to 99.5% at 15 meV energy. The absolute value of the *s*-wave scattering length, A_0 is given by $k^{-1}\tan|\eta_0|$ as $k\rightarrow 0$. Using data in Fig. 9, we find that $A_0 = |24.6| \pm 0.6$ a.u., corresponding to a limiting value of the cross section as $k\rightarrow 0$ of 2130 ± 100 Å^2. The virtual state, associated with the nonadiabatic channel for TNI formation, lies at an energy given by $|(2A_0^2)^{-1}| = 22.5 \pm 1.0$ meV above the zero of energy for the neutral species [59]. This figure appears in good agreement with the theoretical energy estimate of 56 meV in [52], given the complexity of the molecular system involved. This agreement may be somewhat tempered by the subsequent discussion of the vibrational populations of the target (Sec. IV D 3).

2. Determination of the sign of the s-wave scattering-length for C_6F_6

We now describe how our experimental data may be used as good evidence that the sign of A_0 is negative in electron-C_6F_6 encounters, a necessary condition for virtual state scattering. The approximation is introduced that the long-range part of the interaction potential between the electron and C_6F_6 may be described by a charge-induced dipole polarization potential involving some mean static polarizability and varying as r^{-4}. MERT [51,60] then shows that

$$\tan\eta_0 = -A_0 k\left[1 + \left(\frac{4\alpha}{3}\right)k^2 \ln(k)\right] - \left(\frac{\pi\alpha}{3}\right)k^2 + Dk^3 + Fk^4, \tag{8}$$

$$\tan\eta_1 = \left(\frac{\pi\alpha}{15}\right)k^2 - A_1 k^3 + Hk^5, \tag{9}$$

$$\tan\eta_2 = \left(\frac{\pi\alpha}{105}\right)k^2, \tag{10}$$

where α is the mean static polarizability of C_6F_6 (=64.64 a.u. [61]). Equations (8)–(10) yield *s*- and *p* -wave phase shifts which, inserted into Eq. (7), yield integral and backward scattering cross sections. Calculated cross sections could be accurately fitted to experimental data, using A_0, D, F, A_1, and H as fitting parameters. Using a negative value of A_0, excellent consistency could be obtained between integral and backward scattering data, essentially as in Fig. 8. The value of A_0 is found to be −22.9 a.u., 7% lower than in the "partial wave fitting" analysis described above. Absolute values of computed s-wave phase shifts are typically within 1%, or better, of values computed using partial wave fitting, described in Sec. IV D 1. This comparison also shows that we are not in a regime in which there is strong correlation between *s*- and *p*-wave phase shifts, which would suggest that these phase shifts could not be independently determined.

The relative values of individual terms in the MERT expressions, Eqs. (8)–(10), show that analytic terms dominate, at any rate at lower energies, and that terms in higher powers of k , involving the fitting parameters D, F, A_1, and H , make an increasingly lower contribution at lower energy. Thus we have a convergent series in k. In particular, the *p*-wave phase shift remains positive throughout the range of energies considered. The p-wave phase shift also follows the theoretical prescription, shown in Eq. (9), that it should vary linearly with energy at the lowest energies, as shown in Fig. 9.

Returning to Fig. 7, this shows a comparison of the experimental behavior of the ratio R for C_6F_6, CO_2, and C_6D_6, including theoretical values for C_6H_6 [2]. CO_2 and C_6D_6 are systems which show well-characterized virtual state scattering [1,2], and the behavior of R with energy is evidently similar to that for C_6F_6, suggesting a common mechanism for scattering for all three species. In fact, it was shown in [1] that if the variation with energy of the ratio R rises from below 0.5 towards 0.5 at the lowest energies, then A_0 must be negative for the pure elastic-scattering case. Note that this is valid only in the regime in which the dominant terms are the analytic terms in Eqs. (8)–(10), that is, ignoring terms involving D, F, A_1, and H. This condition is met in the case of negative A_0 at energies below 30 meV. In this energy

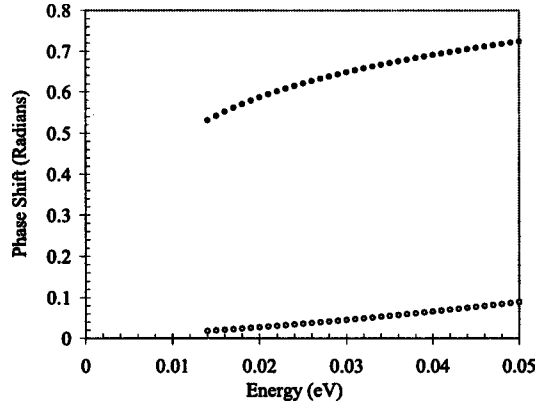

FIG. 9. C_6F_6: *s*-wave (solid circles) and *p*-wave phase shifts (open circles) for $e^- + C_6F_6$ scattering derived from fitting procedures described in the text. Errors associated with the phase shifts are ±5%.

regime, R rises towards 0.5. We conclude, therefore, that $A_0 = -23.75 \pm 1.0$ a.u. to include the range of values obtained by both partial wave and MERT fitting.

To examine further the case for A_0 negative for C_6F_6, we have attempted to fit the C_6F_6 experimental data with a positive value of A_0. Such a fit may be obtained numerically. Terms involving D, F, A_1, and H, however, make the dominant contribution to the phase shifts even at the lowest energies around 15 meV , and no fit to the experimental data is possible without these terms. The p-wave phase shift is in fact found to be negative throughout the energy range because of the dominance of $A_1 k^3$ [Eq. (9)] whereas analytically, that is, omitting the empirical terms of higher order than k^2, η_1 should be positive. Thus attempts to fit with a positive value of the s-wave scattering length result in unphysical behavior.

3. Vibrational populations of the target: C_6F_6

An additional consideration for analysis of C_6F_6 data is that only 21% of the target species occupy the vibrational ground state of the molecule at 300 K. The most heavily populated vibrational levels belong to the e_{2u} and e_{2g} C-C-C bends, respectively 18% and 12% of the total population, e_{1u} C-H bend (9%), and a variety of other motions, b_{2u}, a_{2u}, e_{1g}, and b_{2g}, at the 6–7% level [62,63]. There have been a number of studies of temperature effects in electron collisions with C_6F_6 summarized in [64], which might in principle give some indication of the effect of different vibrational populations. The energy range of data reported in [64] does not extend below 100 meV . At this energy there is a trend for the measured attachment cross sections (as they are termed in [64]) to drop with increasing temperature, falling by a factor of 1.6 between 300 and 575 K.

Nonadiabatic s-wave attachment to e_{2u} vibrational populations of the target is symmetry allowed if the TNI forms in the $^2E_{2u}$ state. According to [52], this state lies 528 meV higher in energy than the lowest $^2A_{1g}$ state. The zero-energy virtual state cross section is given by $2\pi/\Delta E$, where ΔE represents the energy of the virtual state above the energy of the neutral species (see Sec. IV D 1). Thus capture into the $^2E_{2u}$ state would yield a zero energy cross section which is more than an order of magnitude lower than capture into the $^2A_{1g}$ state. Nonadiabatic s-wave attachment involving other vibrational populations is not symmetry-allowed into low-lying states of the TNI, which consist only of $^2A_{1g}$ and $^2E_{2u}$ states. Thus attachment into the virtual state is dominated by the vibrationally unexcited population of the target. This suggests that the cross section for attachment into this population may be approximately five times higher than measured and would correspond to the presence of a virtual state $\sim$10 meV above the zero of energy for the neutral species. These considerations may serve to account for the observed drop with increasing temperature of the attachment cross section reported in [64]; raising the temperature, from 300 to 575 K, causes the vibrationally unexcited population to fall by a factor of 1.9, similar to the fall by a factor of 1.6 in the measured attachment cross section (at 100 meV). In addition, if the measured cross sections for scattering arise from only $\sim$20% of the target species, then interactions may be taking place at considerably longer range than assumed in Sec. IV D 1 and IV D 2. Thus the analysis presented in those sections may need development to include effects of the long-range anisotropic electron-quadrupole interaction.

A further process that can operate is that of superelastic scattering. Consideration of level populations rules out any significant contribution from scattering involving s waves in both input and output channels, since this involves a_{1g} vibrational populations which amount to no more than 1.4% of the total. If we admit an s-wave on the input channel and a p-wave on the more energetic output channel, then superelastic scattering from a_{2u} (at 27 meV) and e_{1u} (at 39 meV) populations is symmetry-allowed either by direct Born-type scattering—since both transitions IR-active—or via the ground-state TNI. The Born process will not contribute more than a few $Å^2$. Scattering via the TNI is also unlikely to be significant because of the small amplitude of the p-wave contribution, and small associated phase shifts, at the low impact energies involved here.

V. CONCLUDING REMARKS

Our conclusions are as follows.

(i) SF_6 and C_6F_6 show qualitatively different behavior with respect to the variation of s-wave phase shift with electron impact energy close to zero impact energy. This is associated with a large positive s-wave scattering length for SF_6 and a large negative value for C_6F_6.

(ii) Data for SF_6 may be analyzed in terms of a combination of electron attachment and elastic scattering. Within the context of a purely electronic description of the scattering, phase shifts may be derived which show the s-wave phase shift rising with decreasing energy. This is analogous to the behavior found for CCl_4 [14].

(iii) Our results are in qualitative agreement with the precepts of theory, as set out in numerous textbooks, e.g., [18]. The exception is that s-wave phase shifts, in both SF_6 and CCl_4 [14] cannot be shown on the basis of the present data to tend towards π as $k \to 0$. This is a necessary condition in order to provide a finite cross section as $k \to 0$ within a purely electronic description.

(iv) The derived low-energy behavior of η_0 poses a theoretical challenge: either the experimental energy is too high at a few meV to probe the regime in which the phase shift rises towards π, or a purely electronic analysis is inappropriate at the collision energies involved. At present we use an asymptotic long-range description of the scattering, which does not include any electronic-nuclear motion coupling—see point (vi) below.

(v) Data for C_6F_6 show that electron scattering at very low energy proceeds via a strong virtual state, with the nonadiabatic $C_6F_6^-$ lying as little as 10 meV above the energy of the neutral. This presents a third example of well-characterized virtual state scattering, the others being CO_2 [1] and benzene [2].

(vi) It would seem likely that many polyatomic systems possess nonadiabatic states of the negative ion, of suitable symmetry, at energies a little above the energy of the neutral. Thus virtual state scattering may well be common among

large polyatomic systems. This has interesting implications which we now briefly mention. Using results in [65], the electronic lifetime of the $C_6F_6^-$ TNI may be estimated, using the present data for the *s*-wave phase shifts, to be ~15 fs at 15 meV impact energy. Incipient nuclear motion may occur in this time and the electronic channel may therefore be regarded as a gateway into electronic-nuclear coupling. This in turn provides a gateway to intramolecular vibrational relaxation with long lifetimes of the resulting TNIs. TNIs may be stabilized either by collisions, in a high-pressure environment, or by IR emission in low-pressure environments, forestalling the ejection of the electron. Both collision or emission yield a mechanism for stable negative ion formation. This process should be significant for industrial plasmas for etching and deposition, in which low-energy electrons abound in the presence of halogenated species, in the atmosphere of the Earth and other planetary atmospheres, and in the interstellar medium, in which electron energies extend down to ~1 meV.

ACKNOWLEDGMENTS

D.F. would like to achnowledge support by the Danish National Research Foundation through the research center ACAP (Aarhus Centre for Atomic Physics) and support from the Danish Natural Science Research Council (SNF). N.C.J. would like to thank the EU EPIC Network for support during the course of this work. J.P.Z. would like to thank the CNRS and SNF for support under the Science Exchange Programme and the EU under the Access to Research Infrastructure Programme (Contract No. HPRI-CT-2001-00122). We would also like to thank the Institute for Storage Ring Facilities at Aarhus (ISA) for providing the facilities necessary for this work.

[1] D. Field, N. C. Jones, S. L. Lunt, and J.-P. Ziesel, Phys. Rev. A **64**, 022708 (2001).
[2] D. Field, J-.P. Ziesel, S. L. Lunt, R. Parthasarathy, L. Suess, S. B. Hill, F. B. Dunning, R. R. Lucchese, and F. A. Gianturco, J. Phys. B **34**, 4371 (2001).
[3] A. Chutjian, A. Garscadden, and J. M. Wadenra, Phys. Rep. **264**, 373 (1995).
[4] D. Klar, M. W. Ruf, and H. Hotop, Int. J. Mass. Spectrom. **205**, 93 (2001).
[5] C. Desfrancois *et al.*, J. Chem. Phys. **111**, 4569 (1999).
[6] R. Parthasarathy, L. Suess, and F. B. Dunning, J. Chem. Phys. **114**, 7962 (2001).
[7] N. C. Jones, D. Field, J.-P. Ziesel, and T. A. Field, Phys. Rev. Lett. **89**, 093201 (2002).
[8] E. Leber, S. Barsotti, J. Bommels, J. M. Weber, I. I. Fabrikant, M. W. Ruf, and H. Hotop, Chem. Phys. Lett. **325**, 345 (2000).
[9] D. Field, G. Mrotzek, D. W. Knight, S. L. Lunt, and J. P. Ziesel, J. Phys. B **21**, 171 (1981).
[10] J. Weiner, V. S. Bagnato, S. Zilio, and P. Julienne, Rev. Mod. Phys. **71**, 1 (1999).
[11] D. Field, S. L. Lunt, and J. P. Ziesel, Acc. Chem. Res. **34**, 291 (2001).
[12] L. Suess, R. Parthasarathy, and F. B. Dunning, J. Chem. Phys. **177**, 11222 (2002).
[13] A. S. Davydov, *Quantum Mechanics*, 2nd ed. (Pergamon Oxford, 1976), pp.495 ff.
[14] J. P. Ziesel, N. C. Jones, D. Field, and L. B. Madsen, Phys. Rev. Lett. **90**, 083201 (2003).
[15] Reference [16] quotes a value of 0.00 eV for the nonadiabatic electron affinity of SF_6. Recent calculations [S.V.K. Kumar (private communication)] show the negative-ion curve crossing the neutral within less than 0.01 Å of the neutral S-F bond length, that is, the negative ion is calculated to be very close to nonadiabatically bound.
[16] L. G . Christophorou and J. K. Olthoff, J. Phys. Chem. Ref. Data **29**, 267 (2000).
[17] E. Tiesinga, A. J. Moerdijk, B. J. Verhaar, and H. Stoof, Phys. Rev. A **46**, R1167 (1992); E. Tiesinga, B. J. Verhaar, and H. Stoof, *ibid.* **47**, 4114 (1993).
[18] R. G. Newton, *Scattering Theory of Waves and Particles*, 2nd ed. (Springer Verlag, New York, 1982).
[19] M. Thoss and W. Domcke, J. Chem. Phys. **109**, 6577 (1998).
[20] E. Gerjuoy and S. Stein, Phys. Rev. **97**, 1671 (1955).
[21] F. B. Dunning, J. Phys. B **28**, 1645 (1995).
[22] J. M. Aje1lo and A. Chutjian, J. Chem. Phys. **65**, 5524 (1976).
[23] A. Chutjian, J. Phys. Chem. **86**, 3518 (1981).
[24] A. Chutjian and S. H. Alajajian, Phys. Rev. A **31**, 2885 (1985).
[25] P.-T. Howe, A. Kortyna, M. Darrach, and A. Chutjian, Phys. Rev. A **64**, 042706 (2001).
[26] D. Klar, M.-W. Ruf, and H. Hotop, Aust. J. Phys. **45**, 263 (1992).
[27] D. Klar, M.-W. Ruf, and J. H. Hotop, Meas. Sci. Technol. **5**, 1258 (1994).
[28] D. Klar, M. W. Ruf, and H. Hotop, Chem. Phys. Lett. **189**, 448 (1992).
[29] A. Schramm, J. M. Weber, J. Kreil, D. Klar, M.-W. Ruf, and J. H. Hotop, Phys. Rev. Lett. **81**, 778 (1998).
[30] J. Ferch, W. Raith, and K. Schröder, J. Phys. B **15**, L175 (1982).
[31] C. D. Finch, R. Parthasarathy, S. B. Hill, and F. B. Dunning, J. Chem. Phys. **111**, 7316 (1999).
[32] L. G. Christophorou and G. Datskos, Int. J. Mass Spectrom. Ion Processes **149/150**, 59 (1995).
[33] O. Ingolfsson and E. Illenberger, Int. J. Mass Spectrom. Ion Processes **149/150**, 79 (1995).
[34] H. Shimamori, T. Sunagawa, Y. Ogawa, and Y. Tatsumi, Chem. Phys. Lett. **227**, 609 (1994).
[35] G. Kasperski, P. Mozejko, and C. Szmytkowski, Z. Phys. D: At., Mol. Clusters **42**, 187 (1997).
[36] H. Cho, R. J. Gulley, K. Sunohara, M. Kitajima, L. J. Ulhmann, H. Tanak, and S. J. Buckman, J. Phys. B **34**, 1019 (2001).
[37] S. V. Hoffmann, S. L. Lunt, N. C. Jones, D. Field, and J.-P. Ziesel, Rev. Sci. Instrum. **73**, 4157 (2002).
[38] G. Martinez, M. Sancho, and F. H. Read, J. Phys. E **6**, 631 (1983).

[39] K. Radler and J. Berkowitz, J. Chem. Phys. **70**, 221 (1979).
[40] K. Rohr, J. Phys. B **10**, 1175 (1977).
[41] R. E. Kennerly, Phys. Rev. A **21**, 1876 (1980).
[42] J. Randell, D. Field, S. L. Lunt, G. Mrotzek, and J. P. Ziesel, J. Phys. B **25**, 2899 (1992).
[43] J-L. Le Garrec, D. A. Steinhurst, and M. A. Smith, J. Chem. Phys. **114**, 8831 (2001).
[44] H. Hotop, D. Klar, J. Kreil, M. W-Ruf, A. Schramm, and J. M. Weber, in *The Physics of Electronic and Atomic Collisions*, edited by L. J. Bubé, J. B.A. Mitchell, J. W. McConkey, and C. E. Brion, AIP Conf. Proc. No. 360 (AIP Press, Woodbury, NY, 1995), p. 267.
[45] Because of the exceptionally large discrepancy between our data and those of Kasperski *et al.* [35], experiments were performed with samples of C_6F_6 obtained from two independent suppliers. Results were the same within experimental error.
[46] L. G. Christophorou and J. K. Olthoff, Int. J. Mass. Spectrom. **205**, 27 (2001).
[47] With regard to attachment cross sections, we note that some recent data [25] report attachment cross sections for electrons with SF_6 which differ at energies of >15 meV from those in [26,44,46] . Our choice of the Kaiserslautern data [26,44] follows discussion with all parties involved.
[48] H. Tachikawa, J. Phys. B **35**, 55 (2002).
[49] D. G. Thompson, Proc. R. Soc. London, Ser. A **294**, 160 (1966).
[50] I. I. Fabrikant and H. Hotop, Phys. Rev. A **63**, 022706 (2001).
[51] T. F. O'Malley, Phys. Rev. **130**, 1020 (1963).
[52] L. N. Shchegoleva, I. V. Beregovaya, and P. V. Schastnev, Chem. Phys. Lett. **312**, 325 (1999).
[53] S. Chowdhury, E. P. Grimsrud, T. Heinis, and P. Kebarle, J. Am. Chem. Soc. **108**, 3630 (1986).
[54] A. Nakajima *et al.*, Chem. Phys. Lett. **214**, 22 (1993).
[55] E. C. M. Chen, J. R. Wiley, C. F. Batten, and W. E. Wentworth, J. Phys. Chem. **98**, 88 (1994).
[56] J. Hernandez-Trujillo and A. Vela, J. Phys. Chem. **100**, 6254 (1996).
[57] G. R. Dennis, I. R. Gentle, and G. L. D. Ritchie, J. Chem. Soc., Faraday Trans. 2 **79**, 529 (1983).
[58] S. L. Lunt, J. Randell, J.-P. Ziesel, G. Mrotzek, and D. Field, J. Phys. B **27**, 1407 (1994).
[59] M. A. Morrison, Phys. Rev. A **25**, 1445 (1982).
[60] S. J. Buckman and J. Mitroy, J. Phys. B **22**, 1365 (1989).
[61] *Handbook of Chemistry and Physics*, edited by R. C. Weast, 66th ed. (CRC, Boca Raton, FL, 1985/1986).
[62] D. Steele and D. H. Whiffen, Trans. Faraday Soc. **55**, 369 (1959).
[63] R. A. R. Pearce, D. Steele, and K. Radcliffe, J. Mol. Struct. **15**, 409 (1973).
[64] P. G. Datskos, L. G. Christophorou, and J. G. Carter, J. Chem. Phys. **98**, 7875 (1993).
[65] D. Field and L. B. Madsen, J. Chem. Phys. **118**, 1679 (2003).